2015

SILICON NANOSTRUCTURES FOR HIGH CAPACITY ANODES IN LITHIUM ION BATTERIES

Tyler M. Selden
Virginia Commonwealth University

SILICON NANOSTRUCTURES FOR HIGH CAPACITY ANODES IN LITHIUM ION BATTERIES

A Thesis submitted in partial fulfillment of the requirements for the degree of Master of Science at Virginia Commonwealth University.

By

Tyler Selden

M.S. Physics

Virginia Commonwealth University 2015

Director: Dr. Ye

Associate Professor, Physics

Virginia Commonwealth University

Richmond, Virginia

December, 2015

Contents

Abstract

SILICON NANOSTRUCTURES FOR HIGH CAPACITY ANODES IN LITHIUM ION BATTERIES

By Tyler Selden MS

A thesis submitted in partial fulfilment of the requirements for the degree of Master of Science at Virginia Commonwealth University.

Virginia Commonwealth University, 2015

Major Director: Dr. Dexian Ye, Associate Professor of Physics

In this study we looked at several different silicon nanostructures grown for the purpose of optimizing anodes for lithium ion batteries. We primarily focused on two distinct types of structures, nanospirals, and Rugate structures. The samples were designed to have the mechanical robustness to endure the massive expansion caused by lithiation of silicon. All of the samples were grown using an electron beam evaporator. Scanning electron microscope images show that we have achieved the desired structural growth. The spirals were shown to have an average diameter of 343 nm on polished copper, and 366 nm on unpolished copper. The Rugate structures had two distinct sample sets. The first mimicked the design of a thin film. The other formed distinct pillars that grouped into islands. The tops of the islands had an average diameter of 362 nm, while the pillars had an average width varying between 167 nm and 140 nm.

List of Figures

Introduction

Lithium ion batteries have become an integral part of consumer electronics and our daily lives. They can power devices ranging from handheld electronics, laptops, even electric and hybrid cars. Lithium ion batteries are preferred over other secondary batteries, lead-acid, nickel cadmium, nickel metal hydride, due to several key properties, such as, high operating voltage, high energy density, low self-discharge rates, and can operate under a wide temperature range [1]. Due to their extensive use, PR Newswire Europe Limited reports that the total sales of lithium ion batteries in 2012 was 11.7 billion USD, and has a projected growth to 33.11 billion USD by 2019 [2]. Not only is the demand for lithium ion batteries increasing, but the demand for higher performance batteries is increasing. The current batteries available fail to meet the United States Department of Energy criteria for energy sources for electric and hybrid vehicles, lacking the specific charge and lifespan required [3], to increase the viability of electric vehicles, the U.S. Department of Energy has issued an initiative to increase the specific energy of batteries from the current 100 Wh/kg to 250 Wh/kg by 2022 [4]. Between the increasing economic demand for lithium ion batteries, and the U.S. Department of Energy's criteria for new higher performance batteries, a redesigned high performance lithium ion battery is highly sought after.

Using recent developments in physical vapor deposition techniques, such as glancing angle deposition, we can create high performance anodes for lithium ion batteries. These anodes

will be mainly comprised of highly porous silicon nanostructures. These nanostructures will allow for reversible insertion and removal of lithium ions from the silicon anode. The structures we created can fall under two broad categories, nanosprings and Rugate structures. These anodes designed using our methodology do not incorporate any binders or scaffolding in the growth process. This will allow for increased charge capacity and ease of scalability. Creating silicon anodes that have near the theoretical charge capacity of silicon, along with cyclability, and ease of scalability, could be a promising development for longer lasting electric devices and vehicles.

Literature Review

Lithium ion Battery History

The lithium ion battery is comprised of three main parts, the cathode, an electrolyte, and the anode. When the battery is discharging, positive lithium ions are moved from the anode, through the electrolyte, and into the cathode. This process releases electrons to be moved through a circuit. While the battery is charging, the positive lithium ions are forced from the cathode, back into the anode. These processes of lithiation and delithiation across the cathode and anode, require that both of the electrodes be comprised of materials that allow for the lithiation/delithiation process to be reversible, as well as stable after many cycles. The first lithium ion battery used transition metal oxides such as $LiCoO_2$ for the positive cathode, and carbonaceous materials as the anode. This type of secondary lithium ion battery was first commercialized in 1991 by Sony [5]. This design of lithium ion battery, transition metal oxide cathode, electrolyte, and carbon based anode, is used today.

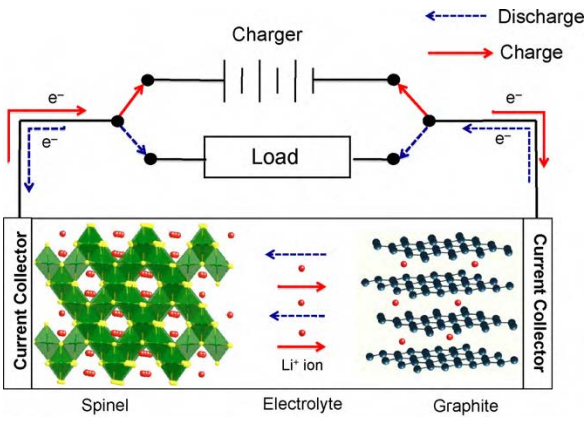

Figure 1 Schematic for Li-ion Battery, with spinel cathode composed of $LiMn_2O_4$

The current anode for lithium ion batteries is generally a carbon material such as graphite. Graphite is a prominent anode material due to its abundance, and high Coulombic efficiency of around 87% [6]. Graphite anodes also exhibit long lifespans in terms of charge

discharge cycles, the average lithium ion battery will still retain 80% of its original charge at the 300th cycle [1]. Carbon based anodes can see such a long lifespan since planar graphite will only undergo a 10% volumetric expansion during the intercalation process [7] . This is due to the fact that there will be only one lithium atom for every six carbon atoms [8] . Because of the small volumetric expansion, stresses due to expansion and contraction of the anode are fairly low, leading to a low probability of stress induced cracking and failure of the carbon anode. However these stresses due to lithiation will eventually cause the graphite anode to crack and fail [9]. The low number of intercalated lithium atoms gives rise to a theoretical capacity for graphite of 372 $mAhg^{-1}$ [7]. Since silicon has a much higher specific charge capacity, 4200$mAhg^{-1}$, we can improve the specific charge density by switching to silicon based anodes [10].

Silicon Review

Silicon is a very promising material to use as an anode material. It is very abundant, silicon makes up 27.7% of the Earth's crust [11]. Along with its abundance, silicon is already well known for its semiconductor properties and use in solar cells, computer chips, and liquid crystal displays. Silicon has now become a promising candidate for an anode material in lithium ion batteries. Silicon has a theoretical charge capacity of 4200 $mAhg^{-1}$ when fully lithiated. Silicon can obtain such high values of charge capacity due to the number of lithium atoms that can be alloyed in silicon, the fully lithiated alloy is $Li_{4.4}Si$ [10]. As lithium atoms are added to the silicon lattice, the lattice will expand. Once the complete alloy is formed, the new fully lithiated alloy will have a fourfold increase in volume as compared to the original silicon lattice [12]. This volumetric expansion can cause severe cracking and ultimately failing of the silicon anode due to the loss of electrical contact. While volumetric expansion will occur for both

crystalline and amorphous silicon, how the lattice changes when lithium is inserted will be different for the two types of silicon.

Silicon Lithiation

When we talk about lithiation of silicon, we can discuss the process in terms of either amorphous or crystalline silicon. The two different types of silicon exhibit different behaviors when dealing with the process of lithiation. These differences will change the performance of anodes based on whether amorphous or crystalline silicon is used.

When crystalline silicon undergoes lithiation, there has been a reported preference to the channel in which the lithium ions will travel. From experimental data, it appears that lithium will first travel through the <110> channel. Seok Woo Lee *et al.* used scanning electron microscopy (SEM) to capture the growth of crystalline silicon nanopillars as they were lithiated. These nanopillars had specific axial orientations, and thus the preferred channel for lithium diffusion could be observed [13]. This finding agrees with the fact that the <110> channel has the lowest energy barrier, since it has the largest distance between neighboring atoms. Along with the preferential growth direction, crystalline silicon is known to go through an irreversible shape change when undergoing lithiation and delithiation. This has been illustrated by the work of Goldman *et al.*, with SEM imaging of crystalline nanopillars before and after cycles of lithiation and delithiation. Their work showed the nanopillars undergo irreversible size transformations, a transition to amorphous silicon, as well as rapid loss in specific charge density [14]. Crystalline silicon has also been shown to form coherent phase boundaries between different concentrations of lithium. These phase boundaries are believed to cause a buildup of internal stress, which leads to premature failure of the nanostructure [15]. These combined effects are believed to be the

cause of rapid decomposition and pulverization of crystalline silicon nanostructures. This breaking of the silicon nanostructures will cause the anodes to fail, resulting in a short battery lifespan. To avoid the disadvantages of crystalline silicon nanostructures, amorphous nanostructures can be used.

Unlike crystalline silicon, amorphous silicon does not have a well ordered long range structure. Instead amorphous silicon is described as continuous random network [16]. This implies that amorphous silicon will have a distribution of bond lengths and channel sizes between nearest neighbors. Huang *et al.* studied the insertion of lithium into amorphous silicon using a ring counting method [17]. They discovered that in low concentrations of lithium, the lithium ions will first reside in lower energy sites, rings that have the furthest separation of nearest neighbors. As more lithium is added to the system, the lithium atoms will begin to insert in less energetically favorable sites. This insertion into the closer packed region will cause volumetric expansion of the silicon lattice [17]. However since this is an amorphous structure, the rings will be randomly orientated, and thus the expansion is isotropic. It is believed that amorphous silicon doesn't form coherent boundaries between different Li_xSi concentrations [18]. Instead amorphous silicon expands plastically [19], due to the constant breaking and reforming of Si-Si bonds [20]. It has also been shown that there may be a critical size for amorphous silicon nanowires where cracking due to volumetric expansion is eliminated. Ryu *et al.* has demonstrated that silicon nanowires with diameters around 300 nm will be extremely resistant to cracking from the lithiation and delithiation process [21]. This is believed to be caused by the uniformity of the pressure gradient across the nanowire [21].

These studies have shown that using amorphous silicon for anode construction is far more advantageous than crystalline silicon. Due to the isotropic expansion, plastic deformation,

and lack of coherent phase boundaries, amorphous silicon anodes will show greater distribution of stress and less cracking than their crystalline counterparts. Therefore, the nanostructures for lithium ion batteries should be fabricated out of amorphous silicon.

Silicon Anodes

In this section we will review some of the many silicon anodes that have been created so that the difference between previous anodes and the ones created for this project will be clear. With this discussion we will highlight the better properties of each design, and state how we plan on incorporating those properties into the nanostructures we developed.

Silicon thin films have been shown to have a very large specific charge capacity. H Jung, and Seung-Ki Joo tested an amorphous silicon thin film, with thickness of roughly 500 Å. This device reached a peak specific charge capacity of 4200 $mAhg^{-1}$, however it failed after only a 20 cycles [22]. This illustrates that a thin film with very small thickness can have extremely high specific charge capacities, however will eventually fail from the stresses caused by lithiation and delithiation.

Silicon nanowires tend to offer better cycling than thin films, as well as a 1D electronic charge pathway for good conductivity [23]. Chakrapani *et al.* grew doped silicon nanowires via chemical vapor deposition on stainless steel, with gold as a catalyst. The nanowires were dopes with either phosphorous or boron to improve electric conductivity. The completed wires had random orientations along the current collector. The wires were measured to have diameters ranging from 80 to 100 nm, and the length of the nanowires was in the order of several hundred micrometers. These wires performed well when a shallow discharge method was used, 1000

$mAhg^{-1}$ at 650 cycles. However at full discharge the capacity and cycling were at 2014 $mAhg^{-1}$ and 50 cycles [24]. Chan *et al.* used a vapor liquid solid deposition technique to create silicon nanowires that were grown unto the current collector, without the use of binders or doping. The nanowires had an average diameter of 89 nm, and initially a crystalline phase of silicon (111). After lithiation the diameters of the nanowires irreversibly increased, and the structure changed to amorphous silicon. The group reports that the specific charge capacity of the nanowires to be 3193 $mAhg^{-1}$ after three cycles, and steady until ten cycles [23]. The authors didn't mention what occurred after ten cycles, whether the anode failed, or some other constraints stopped measurements.

McDowell *et al.* fabricated both crystalline and amorphous nanospheres. They measured a critical diameter, the diameter at which cracks no longer formed from lithiation, for crystalline nanospheres at 150 nm, and no measureable critical diameter for amorphous nanospheres (testing stopped at 870 nm). They concluded that the symmetry of the nanospheres allowed a 2 phase front (expansion and compression) that greatly limited surface stress, allowing for such large diameters of nanospheres without cracking [25].

The use of binders, or coating polymers is a very common practice in silicon anode construction. Lui *et al.* constructed what they called the "pomegranate" design for silicon anodes. This design incorporated single silicon nanoparticle enclosed by a carbon layer. They volume of the enclosed region was sufficient for the volumetric expansion of the silicon nanoparticles upon lithiation. While this battery showed great cyclability, up to 1000 charge/discharge cycles, the specific charge capacity was limited to 1250 $mAhg^{-1}$ [26]. This is due to the added weight of the carbon binders.

While all of these studies show an increase of capacity when compared to a carbon based anode. The various structures all either fail at being able to withstand many cycles of lithiation and delithiation, or they do not reach a high level of charge capacity when compared to the theoretical maximum charge capacity of silicon. While thin films show the highest charge capacity, they offer the lowest number of cycles. Composite binder structures have the highest number of cycles, but the added weight greatly reduces the effective specific charge capacity. Therefore we proposed Rugate structures, and nanospirals as anode devices. Rugate structures should act as a hybrid between nanowires and nanospheres, with the charge capacity and short electron transport of the nanowires, along with the nanospheres ability to disperse stresses from lithiation. Macro springs are already known for their ability to cope with stresses from expansion and contraction, therefore we believe that nanosprings should offer the same resilience to the stresses caused by expansion due to lithiation.

Fabrication and Design Review

Evaporation Process

In order to grow high Rugate structures, and nanosprings, an electron beam (e-beam) evaporator was used in conjunction with glancing angle deposition techniques. An electron beam evaporator is a device in which a direct current of electrons are used to heat a source material. The heated material will turn into a vapor, and then condense on a nearby surface, causing a deposit to form. An e-beam evaporator is generally comprised of four components, the vacuum chamber, a water cooled copper hearth, the electron beam gun, and the substrate [27]. The electron beam gun is a device where electrons are created by a thermionic emission source, then directed either by a voltage potential or magnetic fields. The emitted electrons can be guided to the source material surface by use of magnets, or by line of sight emission [28]. When the accelerated electrons bombard the source material, their kinetic energy will be transferred to the source material as heat. With enough heat added to the source material a phase change will occur, and eventually a gas phase will arise.

The flux of atoms created by the vapor phase will eventually reach the surface of the substrate. At this point nucleation can begin. The first step in nucleation is either absorption unto the surface, or desorption off of the surface. This is determined by the sticking coefficient of the incoming flux. This sticking coefficient is dependent on several factors, such as, the substrate

temperature, the angle of the incoming flux relative to the substrate, and the energy of the incoming flux [28]. Once on the surface, the atoms will have some surface diffusion, depending on the total energy of the incoming atom. The atom will come to rest in a position that minimizes the total energy. After the first layer of atoms are deposited the following atoms follow four basic processes to determine the characteristics of the film. Shadowing can occur, which is a geometric interaction between the roughness of the growing surface and the angular directions of the arriving coating atoms. Surface diffusion, which is the tendency for adatom movement across the surface. Bulk diffusion, which is atomic movement into the surface of deposited material [29].

Glancing Angle Deposition

The growth method used to create the nanostructures in this study was glancing angle deposition. Glancing angle deposition has gained attention in recent years for its ability to create unique, arbitrarily shaped nanostructures [30]. Glancing angle deposition (GLAD) techniques are a form of oblique angle deposition techniques, where extremely high flux angles are used (α>70°). This high deposition angle greatly enhances surface shadowing. Surface shadowing creates areas along the surface, where incoming atoms will not be deposited due to previous structures obstructing their path. The shadowed regions, along with

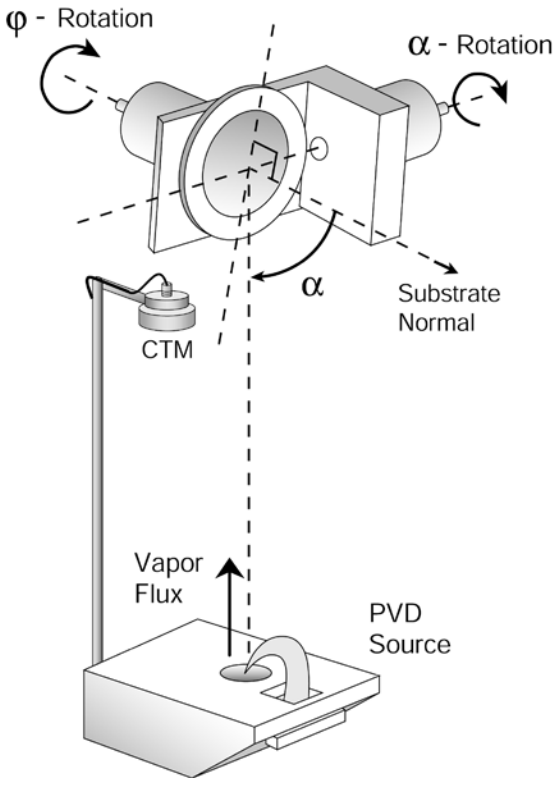

Figure 2 Schematic of a typical GLAD setup

limited adatom diffusion will promote columnar growth on the substrate [31].The columnar growth can then be altered to preferred direction by precise movement of the substrate. If the substrate is rotated during deposition, the columnar growth is nearly normal to the surface. When the substrate is not rotating, the columnar growth is inclined towards the incoming vapor flux. Using various types and degrees of substrate motion during deposition, many exotic nanostructures can be formed. By alternating the substrate 180° at regular intervals, zigzagged structures can be formed, while slow substrate rotation will form helices [32].

Review of Nanospirals

Nanospirals, nanospring, and or helical nanostructures have been developed for several years now and offer a wide range of applications. Copper nanospirals show promise as sensors, catalyst, and energy storage devices [33]. Chemiresistors, or devices that change their electrical properties in the presence of certain chemicals, have been constructed out of silica nanosprings [34]. Nanospirals and nanosprings have also been fabricated for their chiral properties [35]. Along with the many uses of nanospirals and nanosprings, there are many methods available for fabrication. Fabrication techniques include bottom op processes such as glancing angle vapor deposition, vapor phase deposition, soft-template methods, solution chemistry, and top down methods such as lithography, and strain engineering [36]. Zhao *et al.* fabricated square spirals using GLAD. Their procedure used a fixed incident flux angle of 85°, and discrete steps with each subsequent step offset 90° from the previous. These structures were shown to have diameters ranging from 200-500 nm, and a tilt angle of 55°±2° [37]. The width diameter of the spirals can be altered by changing the length of the steps. This leads to some flexibility in designing nanospirals using this type of design. Silicon nanospirals of this nature are great

candidates for lithium ion battery anodes. The symmetry of the spiral, along with the size of the spiral arms should lead to even stress distribution during lithiation and delithiation. Also macroscopic springs exhibit mechanical properties that deal with stress and strain well, therefore nanosprings should exhibit the same behavior.

Review of Rugate Filters

Rugate Filters are a type of interference filter where the refractive index is varied continuously along the depth profile of a thin film, specifically a sinusoidal variation. These can be used in systems to allow the transmittance of selected wavelengths of light, while reflecting others [38]. Typically the fabrication of these devices is done through physical vapor deposition [39]. Brett *et al.* were able to demonstrate the fabrication of titanium dioxide Rugate filters through the use of GLAD. During deposition, the vapor flux incident angle was varied continuously. Since the incident angle is inversely proportional to the density of the film, as the vapor flux incident angle was varied, so was the density of the film. This variation of the density in turn caused the effective refractive index to change, since effective refractive index is dependent on thin film thickness [40]. While the optical properties of this type of Rugate filter are not strikingly important for creating anodes, the ability to create nanorods with spherical sections is. The small width of these individual pillars would have the same benefits as a nanorod, which is already promising anode choice [24]. With a sinusoidal width profile single Rugate pillars would have sections that are spherical in nature, and should alleviate stresses similarly to nanospheres.

Methods and Materials

All of the samples were fabricated in a Cooke electron beam evaporator. This consists of a Telemark Tetratube 10kW power supply, with a Telemark TT controller. Pressure was read by an IGM-400 YCX ionization gauge, controlled by a B-RAX controller. The quartz crystal used for thickness measurements was LeyBold INFICON 6MHz gold coated crystals. Data from the quartz crystal microbalance (QCM) was displayed through an INFICON SQC-310 Thin Film Deposition Controller. All samples were grown on either copper foil or a silicon substrate. The copper foil used was purchased from Matheson Colbian and Bell, and rated at 99.90% copper. The silicon substrate was cut from a silicon wafer supplied by University Wafers, p-type, with <100> orientation. The silicon used for deposition was Alfa Aesar lump silicon, rated at 99.999%. The copper foil was cut into square approximately 4 cm x 6 cm, and polished. A Kristal 620 etching machine was used to polish one side of the copper foil. The polishing solvent used a one to one ratio of water, ethanol, and phosphoric acid. The vacuum chamber had a pressure of 1.84±0.4 micro Torr before deposition.

Simple Spiral

Once placed in the vacuum chamber, the system was pumped down to operating pressure. The first layer of deposition was titanium, with a thickness of 50 nm, at a deposition angle of 13°, and no rotation of the substrate. Titanium was deposited to act as a makeshift titanium

sublimation pump. That is, atomized titanium is very reactive, and will bond with the common gasses in a vacuum chamber to form solid particles, these particles are easier for the system to remove [41]. This reduction of pressure increases the mean free path, which should lead to more control of the nanospirals dimensions. Once the titanium layer was finished, the deposition angle was set to 87°. Now silicon deposition was started, for this deposition process, a warm up cycle had to be completed first, due to the tendency of silicon to spit when its temperature is varied rapidly. The tendency for silicon to spit while having its temperature varied is due to several reasons. The primary reason is believed to be when cold areas of silicon are pulled into the melted region, and rapidly expand. This rapid expansion could cause small droplets of silicon to eject from the melted region [42]. In order to avoid the tendency for silicon to spit, we increased the beam current 5 milliamps every five minutes, from a base current of 15 mA, until a beam current of 85 mA was reached. This gradual increase in temperature was accompanied with a slow and gradual change of the beam position. During the warm up process, silicon would start to melt, and deposition would begin. Each arm had a deposition thickness of 100nm. Once the deposition thickness of 100nm was reached, a stepper motor rotated the substrate by twenty steps. The motor was programmed such that four hundred steps would complete one full rotation, therefore twenty arms creates one layer of the nanospring. After one full rotation was completed, the emission current was stepped down from 85 mA to 15 mA, again using 5 mA steps every five minutes. The substrate was placed at 20° to normal, and 25 nm of nickel was deposited without any substrate rotation. The nickel acts as a conducting agent between each layer of the spiral. The titanium was only deposited as a precursor layer. For the second and following layers, only the processes for silicon and nickel were repeated. This process continued for a total of eight layers.

Rugate Thin Film

The Rugate structure differed from the spirals, in that instead a substrate rotation done in incremental steps, a constant rotation was used with varying substrate angle. The active devices were grown on copper substrate, and a secondary device was grown for imaging, on a silicon substrate. With the copper and silicon substrates loaded into the evaporation chamber, we began the pumping process for the chamber. Once an operational pressure was reached, the substrate angle was placed at 87°. For the first layer, 100 nm of nickel was deposited, with a rotation rate of 0.05 Hz. The nickel was added as a conducting agent, as a binding agent to help cohesion between the silicon and copper, and finally as a protecting layer so lithium ions won't bond with the copper. After the nickel was finished, the substrate angle was moved to 85° and 50 nm of silicon was deposited, keeping the rotation rate at 0.05 Hz. During this deposition process, the beam current was slowly turned up from 15 mA to 85 mA, with a rate of 5mA every 5 minutes. Again this is to avoid the silicon from spitting as the temperature is varied. With 50 nm of silicon completed at 85°, the substrate angle is changed to 75° and another 50 nm of silicon is deposited. At increments of 50 nm of deposited material, the substrate angle was moved to 65°, then 45°, 25°, then reversing the order until 50 nm was deposited at 85. This completed one layer of the Rugate structure. The second layer was started with 25 nm of nickel, deposited at 87°. Then the process described for the first layer was repeated. A total of eight layers were completed.

Rugate Pillar

For this set of Rugate pillars, in order to increase separation between pillars, an initial seeded layer was created. The seeded layer first used a nickel deposition of 50nm at 85°. The

nickel layer was deposited at a rate of 1.5 Angstroms per second, with an emission current of 35 mA. Once this was finished, a layer of silicon at 60° was deposited. For the silicon deposition, the emission current was increased from 15mA to 85 mA using a 5mA increase every 5 minutes. Once the silicon layer was close to completion, the emission current was turned down from 85 mA to 15 mA, using 5 mA steps every 5 minutes. Both layers used a rotation rate of 0.025 Hz. With the seeded layer finished, the Rugate pillars were started. For all layers of the Rugate pillars, a rotation rate of 0.025 Hz was used. The first layer was 50nm of nickel at 86°. This layer had a deposition rate of 1.5 Angstroms per second, using an emission current of 35 mA. With the nickel layer finished, the silicon layers can be started. The substrate was moved to 80° to normal, and the emission current was varied from 15 mA to 85 mA using steps of 5 mA every 5 minutes. With a deposition rate of 1.5 Angstroms per second 150 nm of silicon were deposited at 86°. Keeping the emission current constant, and changing the substrate angel to 80°, 100 nm of silicon was deposited at this angle. The substrate was then moved to 70°, and 50 nm of silicon deposited. The next steps were 30 nm of silicon deposited at 60°, move the substrate to 45° for another 20 nm of deposition. The final step was 20 nm of silicon deposited at an angle of 30°. Once this was completed, the previously mentioned steps were repeated in reverse order, up until 100 nm of silicon deposited at an angle of 80°. After this step begin the cooldown of the silicon, by stepping the emission current from 85 mA to 15 mA. During this process 200 nm of silicon at 86 degrees should be deposited. This process completes one period of the Rugate pillars, this process was repeated for a total of eight times.

Results

Simple Spiral on Polished Copper

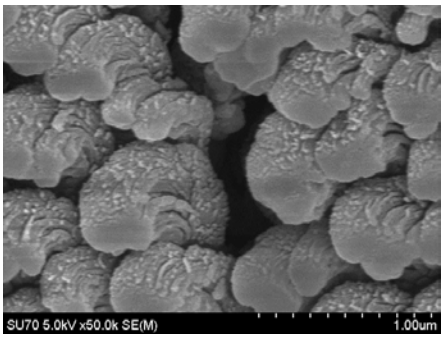

Figure 3: 1 *u*m top down view of nanospirals

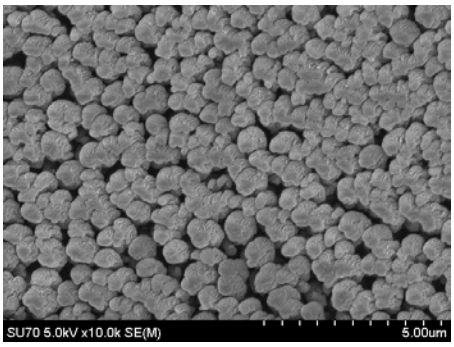

Figure 4: 5*u*m top down view of nanospirals

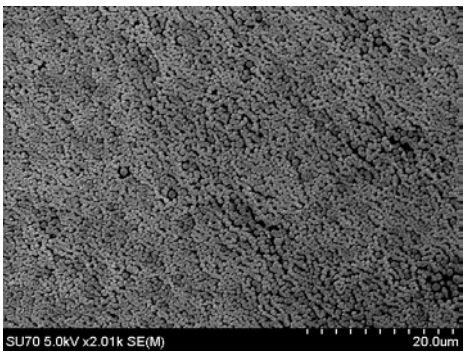

Figure 5: 20 *u*m top down view of nanospirals

The following images were taken using a Hitachi SU-70 scanning electron microscope. From the following images we see that spirals were created using the GLAD technique described above in the methods and materials section. With figure 4 as a reference, ImageJ was used to measure the diameter of the spirals. The average diameter was measured at roughly 343± 32 nm. The smallest diameter recorded was around 88± 32 nm, and the maximum diameter recoded was 691± 32 nm. From the first figure, we can see that each spiral is itself comprised of many small fibers. These fibers were also analyzed using ImageJ. For this sample of nanospirals the fibers were recorded at having an average diameter of 18± 2 nm. The spirals form a highly porous thin film across the structure, from figure 5 we see that the shape is uniform across the surface. Between the diameters of the spirals, and the size of the fibers that the spirals are comprised of, these anodes should allow for good transfer of the lithium ions, by this we mean fast diffusion speed of

the lithium ions through the silicon structure. The fast diffusion speed should lead to more uniform stress gradients within the silicon structure, which will allow for greater durability of the anodes. These lead us to believe that that this type of design would create a highly effective anode for a lithium-ion battery.

Simple Spiral on Unpolished Copper

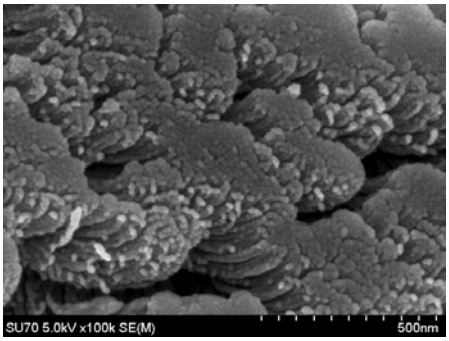

Figure 6: 500 nm top down view of nanospirals

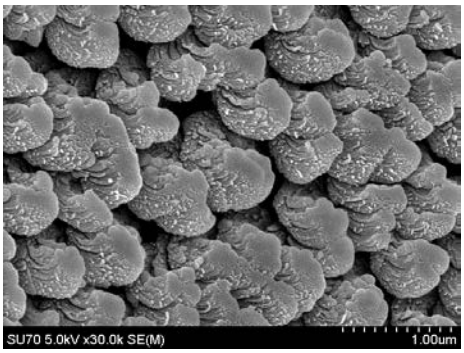

Figure 7: 1 *u*m top down view of nanospirals

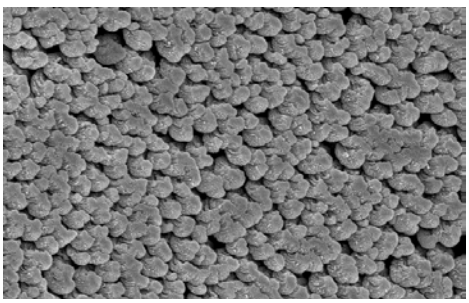

Figure 8: 5 *u*m top down view of nanospirals

The results here are very similar to the polished copper results. Using figure 6 as a reference image in ImageJ, the average diameters was measured at roughly 366 ± 35 nm. The minimum recorded width of one of the spirals was 152± 35 nm, and the maximum recorded diameter was 678± 35 nm. The individual fibers that the spirals are comprised of were also measured using ImageJ. These were measured to have an average diameter of 16± 2 nm. From figure 7, we can see that even on an unpolished copper substrate we have achieved a spiral like structure. From figure 8, the 10 um scale shows that the structure is uniform across the substrate. The thin film created looks to be porous, which should allow ample room for the nanostructure expansion under lithiation. Also the average diameter of the nanostructures is around 300 nm, so the stresses from expansion should be nearly uniform across the nanospirals, therefore it is expected to exhibit good alleviation of the

stresses from lithiation and delithiation. The small fibers shown in figure 6 also suggest these structures will perform well as an anode material, since the small grain size will allow fast lithium transport through the fibers, which again will help the stresses be more uniform across the structure.

Rugate Film

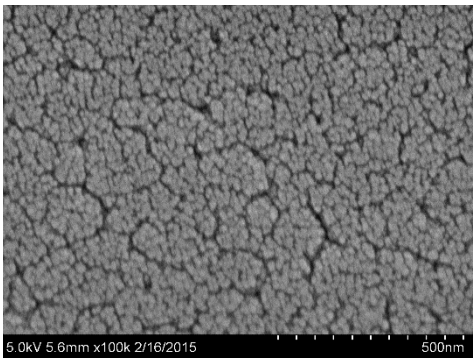

Figure 9: 500 nm overhead view of Rugate Film

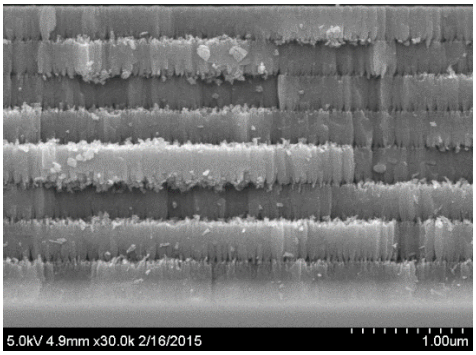

Figure 10: Cross Section of Rugate Film

From all of the SEM images, we can see that the nanostructures have coalesced into a thin film type structure. The overhead image from figure 9, shows that this thin film is uniform across the surface, and lacks porosity. The cross section image figure 10 shows how this structure has a lack of a well-defined sinusoidal width profile, and has coalesced into a thin film type structure. This is most likely attributed to the growth conditions, more specifically the minimum flux incident angle was low enough such that adatom and surface diffusion overcame the shadowing effect from the GLAD procedure. The thin film created is divided into eight layers, each layer corresponding to one period of the width profile. Each layer is 330±15 nm in length. This film may have a high specific charge capacity, but will most likely fail after a few cycles. The lack of porosity leaves no room for the volumetric expansion that will occur during lithiation. This will lead to a buildup of stresses that will eventually crack the film. Once the film cracks too much, lithium ions will not cycle properly.

Rugate Pillar

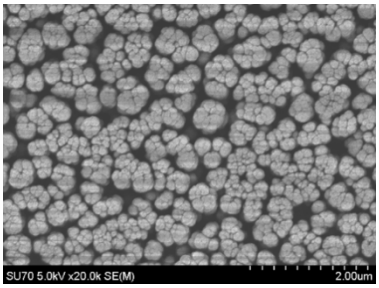

Figure 11: 2 *u*m top down view Rugate Pillar

From the images below, figure 11 shows a 2um top down view of the Rugate structures. From these images we can see that the individual pillars coalesced and formed groups or islands comprised on multiple Nanopillars. Using ImageJ, the diameters of the islands were measured, with an average diameter of 362±25 nm. When observing the cross section image shown in figure 13, we can see the profile of individual pillars. Again using ImageJ, the minimum and maximum diameters, were measured. The average minimum diameter of the Rugate pillars was measured at 140±10 nm. The maximum was measured at 167±10 nm. Figure 13 shows a 5um top down view of the Rugate structures, from this, we can see that the Rugate structures seem fairly uniform across the substrate. Given that the diameter of the islands formed by groups of the Rugate pillars are of small diameter, around 300 nm, along with individual pillar diameters varying between 167 nm and 140 nm, these structures are expected to have good transport speed of lithium ions. The small size means lithium ions will have fast transport speed through the pillars, this means we should see an even distribution of forces caused by the expansion. The sinusoidal profile, with the wider sections being spherical in nature should further reduce some of the stresses caused by lithiation. This leads us to believe that these Rugate structures will work well as anodes for a lithium ion

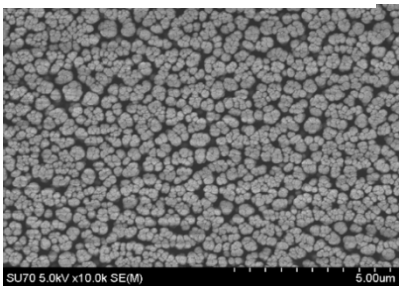

Figure 12: 5 *u*m top down view Rugate Pillar

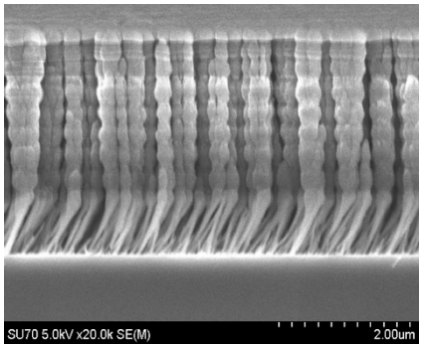

Figure 13: Cross section of Rugate Pillars

battery. However these structures may not have the porosity to allow for the volumetric expansion. Using ImageJ, the total covered area was calculated by tracing the empty spaces. The total covered area was determined to be 80±5%. Using the volume of a conical frustum to model the volume of each island of Rugate pillars, such that

$$V = \frac{1}{3}\pi h(R_1^2 + R_1R_2 + R_2^2) ,$$

where h is the length of the pillar, $R_1$is the average radius at the base, and R_2 is the average radius of the islands. The percent change of the radiuses and length were calculated in order to fill the empty space. If the radiuses and heights are increased by 25%, or a scaling factor of 1.25, the void space will be full. However this only corresponds to a 200% increase in volume, which is below the theoretical increase of 400%. Therefore to compensate for volumetric expansion, it would be recommended that the self-seeding process for these anodes be tailored, so that porosity of the thin film is increased.

Conclusion

From the results section we can see that we have developed three different candidates for high performance anodes for lithium ion batteries. The two different spiral structures that were created (polished, and unpolished substrates) both exhibit similar features. The average diameter, as well as the standard deviation of the average diameter were within a few tens of nanometers of each other. These discrepancies can be overlooked when error is calculated into the results. This shows that the separation between nanospirals created by the shadowing effect from GLAD, had more of an effect on the final structure then the surface morphology of the two copper substrates. This greatly reduced the amount of preparation needed to produce these nanostructures, since polishing copper foil will be unnecessary. Also based on the work done by Ryu *et al.*, these nanospirals should exhibit great cyclability since their diameter is around 300 nm. From their diameter size, and spring structure, these nanospirals are believed to be excellent candidates for anodes in lithium ion batteries.

There were two Rugate structures presented in this work. The first showed little to no porosity, and did not have a sinusoidal width profile. While exhibiting an extremely small feature size, the fact that the structures coalesced into a single thin film, leads us to believe that these structures will not be able to cope with the stresses created by volumetric expansion during lithiation, and therefore would not be a suitable candidate for a lithium ion battery anode. However the second Rugate structure did have all of the qualifying properties for a high performance anode. These structures a diameter around the 300 nm mark, as well as a sinusoidal width profile, which should help alleviate some of the stresses due to expansion similar to

nanospheres. These attributes should lead to an anode that easily handles the stresses created by the volumetric expansion of the lithiation process. However these structures do not meet the porosity requirements for anodes, therefore the spacing between structures should be increased, by tailoring the self-seeding process.

These results have shown that GLAD is a viable technique for creating high performance lithium ion battery anodes. The structures that were fabricated show high porosity, as well as low diameters. The growth method involves few steps, and no preparation of the substrate beforehand. This leads to an easy, scalable fabrication process for potentially high performing silicon anodes.

References

[1] T. Minami and M. Tatsumisago, Solid State Ionics for Batteries, Tokyo: Springer, 2005.

[2] PR Newswire Europe Limited , "Global Lithium Ion Battery Market- Forecast to 2019," PR Newswire Europe Limited, 24 Feb 2014. [Online]. Available: www.researchandmarkets.com/research/4ggxls/global_lithium. [Accessed 12 April 2015].

[3] A. A. Pesaran, T. Markel, H. S. Tataria and D. Howell, "Battery Requirements for Plug-in Hybrid Electric Vehicles-Analysis and Rationale," in *International Electric Vehicle Symposium*, Anaheim, 2007.

[4] B. Cunningham, "Vehicle Technologies Office: Batteries," U.S. DEPARTMENT OF ENERGY, [Online]. Available: http://www.energy.gov/eere/vehicles/vehicle-technologies-office-batteries. [Accessed 2 December 2015].

[5] A. Yoshino, "The Birth of the Lithium-Ion Battery," *Angewandte Essays,* vol. 51, pp. 5798-5800, 2012.

[6] L. Wang, J. Zhao, X. He, J. Ren, H. Zhao, J. Gao, J. Li, C. Wan and C. Jiang, "Investigation of Modified Nature Graphite Anodes by Electrochemical Impedance Spectroscopy," *International Journal of ELECTROCHEMCIAL SCIENCE,* vol. 7, pp. 554-560, 2012.

[7] J. R. Jin , Szczech and Song, "Nanostructured silicon for high capacity lithium battery anodes," *Energy & Environmental Science,* pp. 56-72, 2011.

[8] N. Kambe and M. S. Dresselhaus, "Intercalate Ordering in First Stage Graphite-Lithium," *Material Science and Engineering,* vol. 40, pp. 1-4, 1979.

[9] K. An, P. Barai, K. Smith and P. P. Mukherjee, "Probing the Thermal Implications in Mechanical Degradation of Lithium-Ion Battery Electrodes," *Journal of The Electrochemical Society,* vol. 161, no. 6, pp. 1058-1070, 2014.

[10] E. Hüger, L. Dörrer, J. Rahn, T. Panzner, J. Stahn, G. Lilienkamp and H. Schmidt, "Lithium Transport through Nanosized Amorphous Silicon Layers," *Nano Letters,* vol. 13, pp. 1237-1244, 2013.

[11] The Editors of Encyclopædia Britannica, "Silicon (Si) Chemical Element," Encyclopædia Britannica, 05 02 2015. [Online]. Available: http://www.britannica.com/EBchecked/topic/544301/silicon-Si/278869/Uses. [Accessed 10 04 2015].

[12] W. Wan, Q. Zhang, Y. Cui and E. Wang, "First principles study of lithium insertion in bulk silicon," *JOURNAL OF PHYSICS: CONDENSED MATTER,* vol. 22, 2010.

[13] S. W. Lee, M. T. McDowell, J. W. Choi and Y. Cui, "Anomalous Shape Changes of Silicon Nanopillars by Electrochemical Lithiation," *Nano Letters,* vol. 11, pp. 3034-3039, 2011.

[14] J. L. Goldman, B. R. Long, A. A. Gewirth and R. G. Nuzzo, "Strain Anisotropies and Self-Limiting Capacities in Singe-Crystalline 3D Silicon Microstructures: Models for High Energy Density Lithium-Ion Battery Anodes," *Advanced Functional Materials,* no. 21, pp. 2412-2422, 2011.

[15] L. Y. Beaulieu, T. D. Hatchard, A. Bonakdarpour, M. D. Fleischauer and J. R. Dahn, "Reaction of Li with Alloy Thin Films Studied In Situ ARM," *Journal of the Electrochemical Society,* vol. 11, no. 150, pp. A1457-A1464, 2003.

[16] M. J. Treacy and K. B. Borisenko, "The Local Structure of Amorphous Silicon," *SCIENCE,* vol. 355, pp. 950-953, 2012.

[17] S. Huang and T. Zhu, "Atomistic mechanisms of lithium insertion in amorphous silicon," *Journal of Power Sources,* no. 196, pp. 3664-3668, 2011.

[18] L.-F. Cui, R. Ruffo, C. K. Chan, H. Peng and Y. Cui, "Crystalline-Amorphous Core-Shell Silicon Nanowires for High Capacity and High Current Battery Electrodes," *NanoLetters,* vol. 9, no. 1, pp. 491-495, 2009.

[19] M. Pharr, Z. Sou and J. J. Vlassak, "Measurements of the Fracture Energy of Lithiated Silicon Electrodes of Li-Ion Batteries," *Nano Letters,* vol. 13, no. 11, pp. 5570-5577, 2013.

[20] K. Zhao, W. L. Wang, J. Gregoire, M. Pharr, Z. Sou, J. J. Vlassak and E. Kaxiras, "Lithium-Assisted Plastic Deformation of Silicon Electrodes in Lithium-Ion Batteries: A First-Principles Theoretical Study," *Nano Letters,* vol. 11, no. 7, pp. 2962-2967, 2011.

[21] I. Ryu, J. W. Choi, Y. Cui and W. Nix, "Size-dependent fracture of Si nanowire battery anodes," *Journal of the Mechanics and Physics of Solids,* no. 59, pp. 1717-1730, 2011.

[22] H. Jung, M. Park, Y.-G. Yoon and G.-B. Kim, "Amorphous silicon anode for lithium-ion rechargeable batteries," *Journal of Power Sources,* p. 346–351, 2003.

[23] C. K. Chan, H. Peng, G. Liu, K. McIlwrath, X. F. Zhang, R. Huggins and Y. Cui, "High-performance lithium battery anodes using silicon nanowires," *Nature Nanotechnology,* vol. 3, pp. 31-35, 2008.

[24] V. Chakrapani, F. Rusli, M. A. Filler and P. A. Kohl, "Silicon nanowire anode: Improved battery life with capacity limited cycling," *Journal of Power Sources,* no. 205, pp. 433-438, 2012.

[25] M. Mcdowell, S. W. Lee, J. T. Harris, B. A. Korgel, C. Wang, W. D. Nix and Y. Cui, "In Situ TEM of Two-Phase Lithiation of Amorphous Silicon Nanospheres," *Nano Letters,* vol. 13, no. 2, pp. 758-764, 2013.

[26] N. Lui, Z. Lu, J. Zhao, M. T. McDowell, H.-W. Lee, W. Zhao and Y. Cui, "A pomegranate-inspired nanoscale design for large-volume-change lithium battery anodes," *Nature Technology,* vol. 9, no. 3, pp. 187-192, 2014.

[27] J. Singh and D. E. Wolfe, "Review Nano and macro-structured component fabrication by electron beam-physical vapor deposition (EB-PVD)," *Journal of Materials Science,* vol. 40, pp. 1-26, 2005.

[28] C. Bishop, Vacuum Deposition onto Wbs, Films, and Foils, Oxford: Elsevier, 2011.

[29] J. A. Thornton, "High Rate Thick Film Growth," *Annu. Rev. Mater Sci,* vol. 7, pp. 239-260, 1977.

[30] C. Patzig, T. Karabacak, B. Fuhrmann and B. Rauschenbach, "Glancing angle sputter deposited nanostructures on rotating substrates: Experiments and simulations," *Journal of Applied Physics,* vol. 104, no. 094318, pp. 1-9, 2008.

[31] M. W. Seto, B. Dick and M. Brett, "Microsprings and microcantilevers: studies of mechanical responce," *Journal of Micromechanics and Microengineering,* vol. 11, pp. 582-588, 2001.

[32] K. Robbie and M. Brett, "Sculptured thin film and glancing angle deposition: Growth mechanics and applications," *Journal of Vacuum Science and Technology A,* vol. 3, no. 15, pp. 1460-1465, 1997.

[33] L. Chen, L. Andrea, Y. Timalsina, G.-C. Wang and T.-M. Lu, "Engineering Epitaxial-Nanospiral Metal Films Using Dynamic Oblique Angle Deposition," *Crystal Growth and Design,* no. 13, pp. 2075-2080, 2013.

[34] V. Dobrokhotov, L. Oakes, D. Sowell, A. Larin, J. Hall, A. Kengne, P. Bakharev, G. Corti, T. Cantrell, T. Prakash, J. Williams and D. Mcllroy, "ZnO coated nanospring-based chemiresistors," *Journal of Applied Physics,* vol. 111, no. 044311, 2010.

[35] E. Schubert, J. Fahlteich, T. HöcheŽŸ, G. Wagner and B. Rauschenbach, "Chiral silicon nanostructures," *Nuclear Instruments and Methods in Physics Research B,* no. 244, pp. 40-44, 2006.

[36] Z. Ren and P.-X. Gao, "A review of helical nanostructures: growth theories, synthesis strategies and properties," *Nanoscale,* vol. 6, pp. 9366-9400, 2014.

[37] Y. -P. Zhao, D. -X. Ye, G. -C. Wang and T. -M. Lu, "Designing Nanostructures by Glancing Angle Deposition," in *SPIE Vol. 5219 Nanotubes and Nanowires*, Bellingham, 2003.

[38] H. A. Macleod, Thin-Film Optical Filter, Bristol: Institute of Physics Publishing, 2001.

[39] N. k. Sahoo, S. Thakur and R. B. Tokas, "Superior refractive index tailoring properties in composite ZrO2/SiO2 thin film systems achieved through reactive electron beam codeposition process," *Applied Surface Science,* no. 253, pp. 618-627, 2006.

[40] A. van Popta, M. M. Hawkeye, J. C. Sit and M. J. Brett, "Gradient-index narrow-bandpass filter fabricated with glancing-angle deposition," *Optics Letters,* vol. 29, no. 21, pp. 2545-2547, 2004.

[41] D. J. Harra, "Review of sticking coessicients and sorption capacities of gases on titanium films," *Journal of Vacuum Science & Technology,* no. 13, pp. 471-474, 1976.

[42] M. L. Rappaport and B. Berkovitz, "A graphite crucible for spitting-free high rate e-gun evaporation of Ge," *Journal of Vacuum Science & Technology,* no. 21, p. 102, 1982.